

Emergence of Protoplanetary Disks and Successive Formation of Gaseous Planets by Gravitational Instability

Shu-ichiro Inutsuka¹, Masahiro N. Machida², and Tomoaki Matsumoto³

ABSTRACT

We use resistive magnetohydrodynamical simulations with the nested grid technique to study the formation of protoplanetary disks around protostars from molecular cloud cores that provide the realistic environments for planet formation. We find that gaseous planetary-mass objects are formed in the early evolutionary phase by gravitational instability in regions that are decoupled from the magnetic field and surrounded by the injection points of the magnetohydrodynamical outflows during the formation phase of protoplanetary disks. Magnetic decoupling enables massive disks to form and these are subject to gravitational instability, even at ~ 10 AU. The frequent formation of planetary-mass objects in the disk suggests the possibility of constructing a hybrid planet formation scenario, where the rocky planets form later under the influence of the giant planets in the protoplanetary disk.

Subject headings: magnetohydrodynamics —ISM: jets and outflows —stars: formation —stars: low-mass, brown dwarfs —stars: planetary systems: protoplanetary disks —stars: planetary systems: formation

1. Introduction

Recent direct imaging of outer planets in extra-solar planetary systems (Kalas et al. 2008; Marois et al. 2008; Lagrange et al. 2008; Greaves, J. S. et al. 2008; Thalmann et al. 2009) provides a challenging question to the theory of planet formation: how are giant planets formed in the distant regions far from the central star? Almost all the dynamical

¹Department of Physics, Nagoya University, Furo-cho, Chikusa-ku, Nagoya, Aichi 464-8602, Japan; inutsuka@nagoya-u.jp

²National Astronomical Observatory, Mitaka, Tokyo 181-8588, Japan; masahiro.machida@nao.ac.jp

³Faculty of Humanity and Environment, Hosei University, Fujimi, Chiyoda-ku, Tokyo 102-8160, Japan; matsu@i.hosei.ac.jp

timescales for the various important processes in planet formation essentially scale with the Kepler rotation timescale (e.g., Kokubo & Ida 2002). In the standard core-accretion scenario, there are severe timescale constraints on the in situ formation of Jovian planets, even at 5 AU from the central star (e.g., Pollack et al. 1996; Ikoma, Nakazawa, & Emori 2000; Hubickyj et al. 2005; Hori & Ikoma 2008; Lissauer et al. 2009; Machida et al. 2010). Consequently, the formation of planets at greater distances (up to $\sim 10^2$ AU) seems to be impossible within an observationally reasonable timescale in the core-accretion scenario of planet formation (e.g., Ida & Lin 2004). On the other hand, the formation of giant planets due to gravitational instability of massive protoplanetary disks has been extensively investigated by various authors (e.g., see review by Durisen et al. 2007). However, most analyses focused only on the evolution of hypothetical disks and cannot be applied directly to actual systems. The result of gravitational instability or absence of it does depend on how the protoplanetary disks are formed, but the formation of the protoplanetary disk is closely related to the formation of the central star. In other words, the initial conditions of planet formation by gravitational instability should be provided by the star formation process.

The last decade has seen dramatic progress in our understanding of protostar formation (e.g., André et al. 2008) and now provides us with the opportunity to study the formation phase of protoplanetary disks. A highlight of the recent non-ideal magnetohydrodynamical (MHD) calculations of protostellar collapse from molecular cloud cores is the driving of outflows from the first cores and well-collimated fast jets from the protostars; these may be regarded as proof of the importance of various physical processes such as the ohmic dissipation of magnetic fields due to the low degree of ionization at higher density phases. In this Letter, we study the formation phase of protoplanetary disks in a self-consistent, non-ideal MHD system. Our protostellar collapse calculations start from a molecular cloud core, include (practically) all the realistic physical processes, and show how knowledge of the protostar formation process provides convincing evidence for the formation of giant planets in the early phase.

2. Non-Ideal MHD Simulations

The initial condition of our resistive MHD simulation is the critical Bonner-Ebert Sphere (an isothermal sphere at gravitational equilibrium) with a temperature of 10 K and a radius of 4750 AU. In order to initiate gravitational collapse, we increase the density uniformly by a factor of 3 to an initial central density of $3 \times 10^6 \text{ cm}^3$. The mass is 1.6 times the solar mass. In a typical simulation, we use a uniform rotation of the angular velocity of $\Omega_{\text{init}} = 1.1 \times 10^{-13} \text{ s}^{-1}$ and a uniform magnetic field strength of $B_{\text{init}} = 37 \mu \text{ G}$ in the initial state. The initial ratios

of thermal, rotational, and magnetic energy to the negated gravitational energy are 0.3, 0.005, 0.014, respectively (cf., Machida et al. 2008c). We adopt the nested-grid scheme in order to increase the spatial resolution of the central region (Machida et al. 2005); the number of nest-grids is typically 12 and each grid has $n_x \times n_y \times n_z = 128 \times 128 \times 32$ cells (Machida et al. 2006c). As a result, spatial resolution of the innermost grid is 0.58AU and that of the outermost grid is 1200AU.

To describe a realistic evolution of the magnetic field in protostar formation, we should take into account the non-ideal MHD effects of weakly ionized molecular gas. In general, the ambipolar diffusion is important in the low-density phase, but it is slow and not critical in the dynamically collapsing state. In the intermediate-density phase, the Hall term effect can produce a modest effect depending on the size distribution of dust grains (Wardle & Ng 1999). In contrast, ohmic dissipation dominates in the high-density phase, and is shown to be the most efficient mechanism for the dissipation of magnetic field in the magnetically supercritical cloud core (e.g., Nakano et al. 2002). Therefore, we model the non-ideal effects of the magnetic field by the effective resistivity in the induction equation. We adopt the resistivity evolution of the fiducial model of Machida et al. (2007) that corresponds to the ionization equilibrium in standard molecular clouds. As the cloud core collapses, the degree of ionization decreases with increasing density. The gas becomes magnetically decoupled at densities of around 10^{10}cm^{-3} but couples again when the temperature exceeds about 1000 K. The adopted equation of state is the same as that used in Machida et al. (2009) that follows the radiation hydrodynamical calculations of protostellar collapse (Masunaga & Inutsuka 2000).

3. Results

Figure 1 shows a typical “bird’s eye-view” snapshot of our simulations. The timescale of the gravitational collapse (i.e., free-fall time) is a decreasing function of density; therefore, the dense central region shrinks faster than the less-dense surrounding regions. This property of gravitational collapse almost always leads to the successive decrease of mass inside the faster shrinking region in a run-away manner. This gravitational “run-away collapse” is decelerated by a gradual increase in the temperature of the central region, and eventually a quasi-steady object called “the first core” is formed (Larson 1969; Winkler & Newman 1980a,b; Masunaga et al. 1998). It consists mainly of hydrogen molecules and has a radial extent exceeding 10 AU. The molecular gas surrounding the first core continues to accrete onto it, resulting in a slow but monotonic increase in density and temperature at the center of the first core. If the initial angular momentum of the molecular cloud core is on the

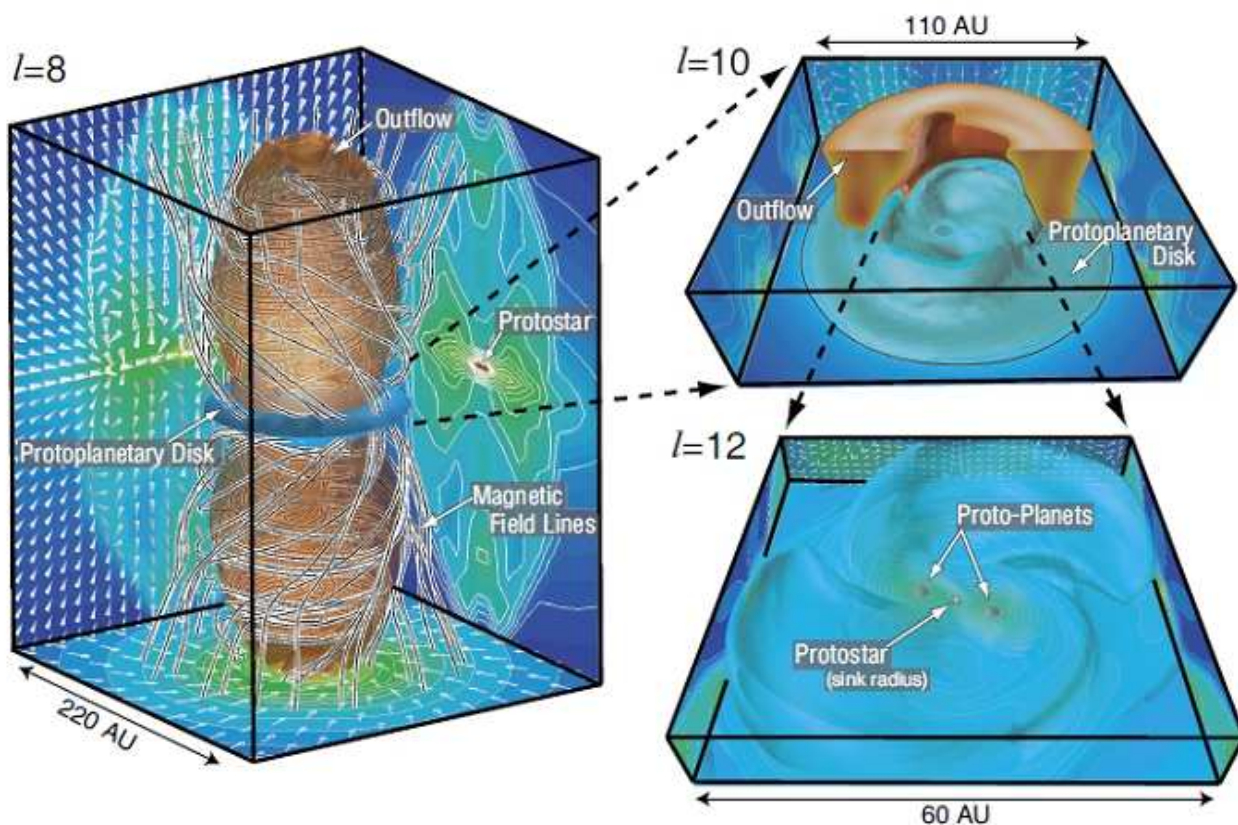


Fig. 1.— Bird’s eye-view of the result of non-ideal MHD simulation with nested grid technique, covering the evolution of the molecular cloud core to the protostar. The left panel shows the structure in the grid, level $l = 8$, where the high-density region ($n = 10^{10}\text{cm}^{-3}$; blue isodensity surface) and magnetic field lines are plotted. Two cocoon-like structures (brown) above and below the flattened core denote the zero-velocity surface inside of which the gas is outflowing from the center. The density contours (color and contour lines) and velocity vectors (thin white arrows) are projected in each wall surface. The right upper panel shows the structure in part of the 10th grid, where we can clearly see the central cavity in the outflowing region. The right lower panel (12th grid) shows the protoplanetary disk in the formation phase, and two newly formed planetary-mass objects in the disk.

order of the value suggested by observation, the resultant first core rotates significantly fast, and its formation corresponds to the onset of bipolar outflows driven by magnetic fields (Tomisaka 2002; Machida et al. 2006a; Banerjee & Pudritz 2006; Machida et al. 2008a; Hennebelle & Fromang 2008). In Figure 1, the outflow regions are shown by the two brown cocoon-like structure that correspond to the zero vertical velocity surfaces ($v_z = 0$): gas inside the cocoons has a significant vertical velocity.

Most of the angular momenta in gravitationally collapsing objects are removed by the Maxwell stress of the field, which is called magnetic braking (Machida et al. 2007). In addition the outflowing gas carries away angular momentum during this phase. When the central temperature becomes sufficiently high ($\sim 2 \times 10^3\text{K}$), the dissociation of hydrogen molecules becomes significant, providing effective cooling that makes the core gravitationally unstable, triggering “the second collapse” (Masunaga & Inutsuka 2000; Machida et al. 2006a, 2007, 2008a).

The upper right panel of Figure 1 shows an enlarged view of the region inside the outflow-launching regions, where the resistivity is so significant that the magnetic field is decoupled from the gas. The outflow region envelopes the “dead zone” for magnetic field (Machida et al. 2008a) where magnetic braking is not operating. Therefore, the infalling gas in the first core maintains angular momentum and reaches the radius of the centrifugal barrier to form a circumstellar disk-like structure. The formation of this disk-like structure corresponds to the birth of the protoplanetary disk, which happens inside the outflow-launching region.

The infalling from the envelope to the central region continues, and the radius of the outflow-launching region increases over time, as does the outer boundary of the magnetic dead zone. Likewise, both the mass and the outer radius of the circumstellar disk increase over time. Eventually, the radius of the disk extends beyond the initial radius of the first core and the first core disappears; in other words, the first core transforms itself into a protoplanetary disk.

An important consequence of the early formation of the protoplanetary disk is the gravitational fragmentation of the disk and the formation of planetary-mass objects, as shown in the lower right panel of Figure 1. The reason for the gravitational instability can be understood in terms of the ratio of the disk mass to the central object. Figure 2 shows a schematic evolution of protostellar objects, in terms of mass. The vertical axis denotes mass (in units of solar mass) and the horizontal axis denotes time (in units of year). The red curve on the left-hand side depicts the mass of the fast collapsing region in the center of the molecular cloud core in the first collapse phase, which essentially defines the gravitationally unstable mass, and thus, corresponds to the Jeans mass. The decrease of this mass in the isothermal phase describes the run-away collapse of central region, a

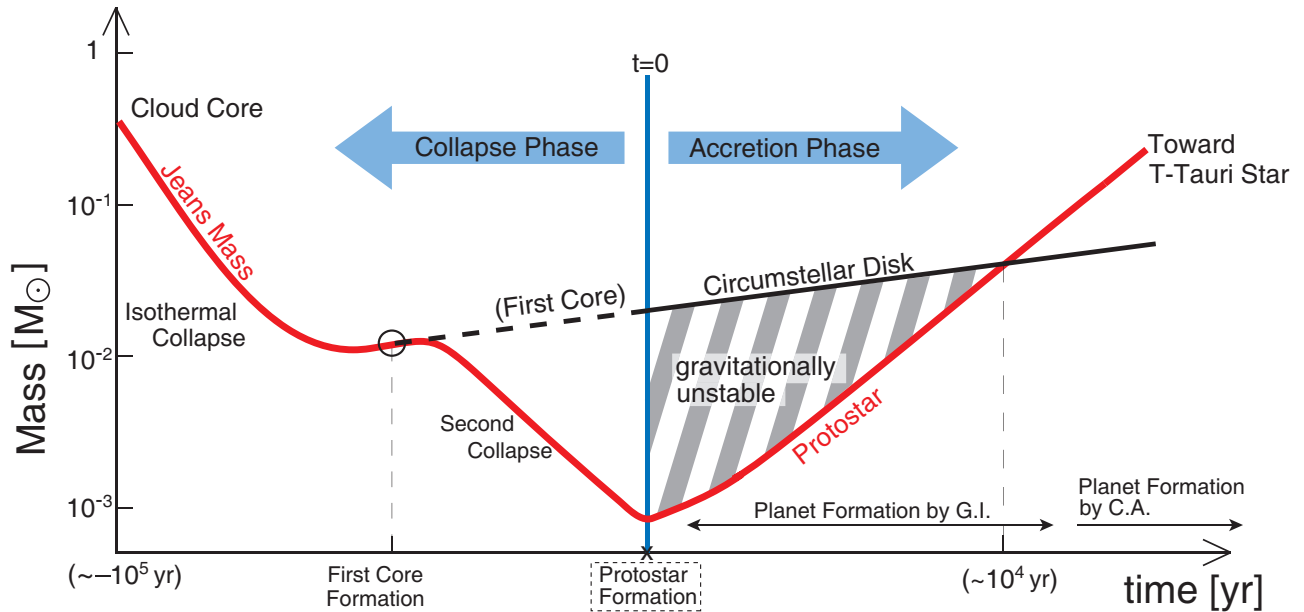


Fig. 2.— Schematic diagram for the evolution of protostellar objects, in terms of mass. The vertical axis denotes mass (in units of solar mass) and the horizontal axis denotes time (in years). The red curve on the left-hand side depicts the mass of the fast collapsing region in the center of the molecular cloud core in the collapsing phase, which essentially defines the gravitationally unstable mass, and therefore corresponds to the Jeans mass. Note that the mass of the first core is much larger than the mass of the central protostar at its birth. The right-hand side describes the evolution in the main accretion phase, where gas in the envelope of the molecular cloud core accretes onto the central region and the protostar gains its mass. As the first core gradually changes into the protoplanetary disk, the mass of the protoplanetary disk remains larger than the mass of the protostar for a while. This configuration is gravitationally unstable and creates self-gravitating objects in the disk. The protostar mass increases monotonically and overwhelms the mass of the disk later in the accretion phase.

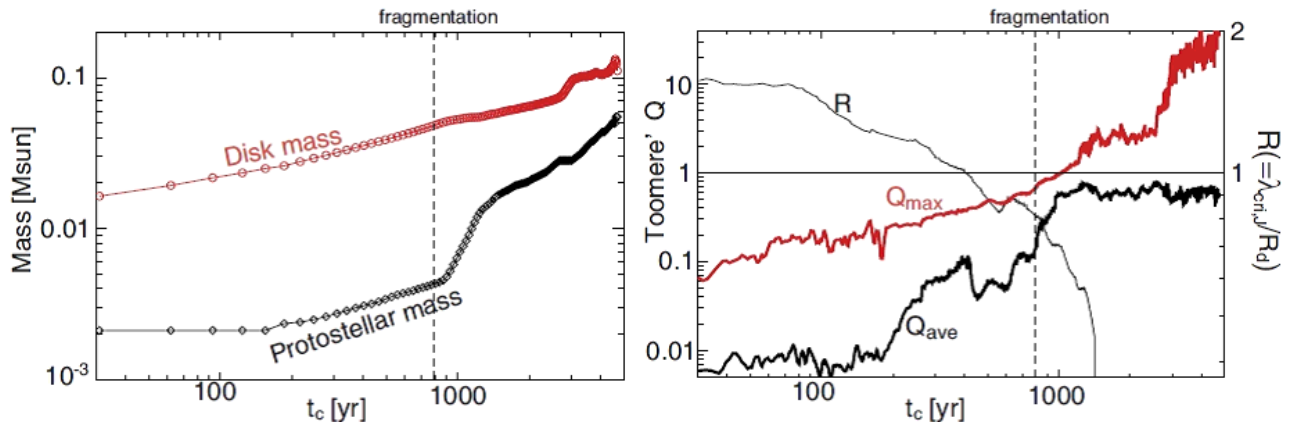


Fig. 3.— Left panel shows actual evolution of protostar mass and disk mass, where the horizontal axis denotes elapsed time in years after the formation of the protostar. The right panel shows time evolution of the gravitational instability indicator $Q \equiv \kappa C_S / (\pi G \Sigma)$. Q_{max} is the maximum value in the disk and Q_{ave} is the average value. The curve labeled R denotes the ratio of the most unstable wavelength to the disk radius. At $t \approx 800$ yr, R becomes smaller than unity so that the gravitationally unstable mode is possible in the disk, and planetary-mass objects are formed.

characteristic of gravitational collapse of cooling gas. The slight increase of the central mass (the Jeans mass) corresponds to the formation of the first core and its gradual increase in a quasi-steady state. The second fall of the central mass corresponds to “the second collapse” that is triggered by the endothermic dissociation of hydrogen molecules. After most of the hydrogen molecules are dissociated, the adiabatic increase in the pressure of the atomic gas eventually overcomes the gravitational collapse and the second core forms. Therefore, the decrease of the central mass in the second collapse stage is closed by the formation of a protostar. We should note that the mass of the first core is much larger than the mass of the central protostar at its birth.

The right-hand side of Figure 2 describes the evolution in the main accretion phase, where gas in the envelope of the molecular cloud core accretes onto the central region and the protostar gains mass. As the first core gradually changes into the protoplanetary disk, the mass of the protoplanetary disk remains large (and even larger than the protostar) for a while. This configuration is gravitationally unstable and the spiral arms are excited, which promotes gas accretion in the disk, but the accretion is not efficient enough to avoid gravitational fragmentation of the disk, creating self-gravitating objects in the disk. The typical mass of the formed objects is a fraction of the disk mass (i.e., smaller than 10^{-2} solar masses) which corresponds to the range of Jovian planets to brown dwarfs. The protostar

mass increases monotonically and eventually overwhelms the mass of the disk. In effect Figure 2 describes why and how the gravitationally unstable protoplanetary disk is created.

The left panel of Figure 3 shows the actual evolution of the protostar mass and disk mass, where the horizontal axis denotes elapsed time (in years after the formation of the protostar). The right panel shows the time evolution of the indicator of gravitational instability $Q \equiv \kappa C_S / (\pi G \Sigma)$, where κ , C_S , G , and Σ are epicyclic frequency, sound speed, gravitational constant, and surface density, respectively. Q_{\max} is the maximum value in the disk and Q_{ave} is the average value. During the first several hundred years, Q remains smaller than unity and the disk satisfies the instability criterion obtained by local linear analysis, although the size of the disk remains too small for the unstable mode to appear, as shown by the curve labeled R that denotes the ratio of the most unstable wavelength to the disk radius. At $t \approx 800$ yr, R becomes smaller than unity so that the gravitationally unstable mode becomes feasible in the disk; this epoch does indeed correspond to the fragmentation of the disk. Note that the fragmentation has occurred in the region where the effective equation of state is almost adiabatic. If additional radiative cooling operates, it will become even more unstable, and thus, the fragmentation is definitely expected. In other words, the gravitational fragmentation shown in this early formation phase of the massive disk does not require efficient radiative cooling that is supposed to be important in the later phase of the evolution where the disk is less-massive and less-unstable (e.g., Gammie 2002; Rice et al. 2003, 2005). Here we emphasize that we should expect the growth of gravitational instability in the disks that excessively satisfy the local instability criterion ($Q < 1$) for the mode whose wavelength is sufficiently smaller than the disk. Nevertheless, the consequence of the growth and the resultant fragmentation should be studied in more detail including the effect of irradiation from the central star that is not taken into account in the present calculations.

The formation of planetary-mass objects and the excited spiral arm structure provide an efficient transfer of angular momentum in the disk and promote mass accretion onto the protostar, as shown by the rapid increase in the protostar mass in the left panel. This property will be further investigated in our next paper.

4. Discussion

Cooling Efficiency Since we are not solving realistic radiative transfer equation in our dynamical simulations, one might wonder whether each fragment can sufficiently shrink by radiating an excess energy obtained by compressional heating or not. Here we estimate the amount of energy that should be radiated away from a fragment and compare with the cooling capability of the fragments. In order for the self-gravity to dominate over gas pressure the

effective ratio of specific heats (γ_{eff}) should be less than 4/3, while the ratio of specific heats (γ) for the molecular gas in adiabatic evolution is mostly 7/5 (e.g., Masunaga & Inutsuka 2000). Thus, we can roughly calculate the amount of energy ΔE that should be radiated during the compressional motion of the planet with mass M_p from the density ρ_d , pressure P_d , and temperature T_d in the gas disk to the average density ρ_p and pressure P_p of the planet as,

$$\Delta E = \frac{M_p}{\gamma - 1} \left(\frac{P_d}{\rho_p} \right) \left[\left(\frac{\rho_p}{\rho_d} \right)^\gamma - \left(\frac{\rho_p}{\rho_d} \right)^{\gamma_{\text{eff}}} \right]. \quad (1)$$

If we take the density enhancement factor of 10^5 (e.g., $\rho_d = 10^{-11} \text{g cm}^{-3}$ and $\rho_p = 10^{-6} \text{g cm}^{-3}$) the second term is negligible compared to the first term on the right-hand side of the above equation. Thus, the expected time-averaged luminosity of the fragment that cools with the timescale Δt can be calculated as,

$$\langle L \rangle \equiv \frac{\Delta E}{\Delta t} \approx 1.5 \times 10^{-1} \left(\frac{M_p}{10^{-3} M_\odot} \right) \left(\frac{T_d}{10^2 \text{K}} \right) \left(\frac{10^2 \text{yr}}{\Delta t} \right) \left(\frac{\rho_p}{10^5 \rho_d} \right)^{2/5} L_\odot, \quad (2)$$

where we assumed that the mean molecular weight is 2.3. On the other hand, the luminosity L_p of the planet with radius R_p and the surface temperature T_p is

$$L_p = 4\pi R_p^2 \sigma_{\text{SB}} T_p^4 = 1.9 \times 10^{-1} \left(\frac{R_p}{10^{12} \text{cm}} \right)^2 \left(\frac{T_p}{10^3 \text{K}} \right)^4 L_\odot, \quad (3)$$

where σ_{SB} is Stephan-Boltzmann constant. Since $(T/T_d) = (\rho/\rho_d)^{\gamma_{\text{eff}}-1}$, compression by a factor of $\rho_p/\rho_d = 10^5$ with $\gamma_{\text{eff}} = 4/3$ results in the increase of temperature by a factor of about 46. Thus, the fragment can radiate efficiently enough to collapse gravitationally by a factor of at least 10^5 in density within 100 years (i.e., the resultant surface temperature of the planet will be somewhat smaller than 10^3K). Thus, the objects formed by the gravitational instability of the disk as in our simulation are expected to be dense enough to avoid being washed out in the dynamical environment.

Further Evolution What is the fate of these gravitationally formed planetary-mass objects? Does gravitational interaction with the gaseous disk lead to the migration of these objects? In fact, some of our simulations showed the objects falling into the central star, while in other cases they migrated outward but remained in the disk. Their chaotic behavior is not surprising, since eccentricities of the orbits of planetary-mass objects in the disk are, in general, not small. Their large eccentricities are due to the fact that they absorb infalling gas.

In addition, the gravitational fragmentation and formation of planetary-mass objects repeat many times during the main accretion phase, where the gas accretion from the envelope of the molecular cloud core continues. Some of the planetary-mass objects fall onto

the central star while some remain in the disk. Therefore, a statistical method seems to be required to predict the distribution of objects that survive the gas dispersal, which will be the scope of our subsequent paper.

Implication for Observations Astronomical observation of the early formation phase of protoplanetary disks would enable us to directly test these expectation. Although our numerical simulations enable us to frequently observe the gravitational fragmentation of protoplanetary disks, in reality this process is hidden in dense gas and may remain invisible in optical and near-infrared wavelengths. However, radio interferometers are potentially capable of observing the interiors of protostellar cloud cores. The Atacama Large Millimeter Array (ALMA) would be an ideal tool for this type of observation. In order to directly observe the process described in this Letter, it is necessary to observe the early evolutionary phase within about 1000 years from the birth of a protostar. As the average lifetime of a protostar is estimated to be 10^5 year, the required time span for this observation is only 1 % of the protostar’s lifetime, meaning that we should observe, on average, about 100 protostars to find one protostar at an early evolutionary phase. In our simulations, we almost always observe very time-dependent mass accretion through the gravitationally unstable disk. Therefore, another possible observational signature is the time variability of the protostellar source. We hope that the gravitational fragmentation reported in this Letter will be analyzed observationally and a realistic planet formation scenario will be refined in the near future.

The frequent formation of planetary-mass objects in the disks during the formation phase suggests that we should consider their influence on the evolution of the protoplanetary disk. In particular, it suggests a new possibility for the core-accretion scenario in the region outside the orbit of the planetary-mass object where the shepherding effect from a massive object prevents dust grains from raining out onto the central star (Muto & Inutsuka 2009), which corresponds to the far right-side of Figure 2. Therefore, it might be interesting to search for a hybrid scenario of planet formation where the rocky planets form after the gravitational formation of the gaseous giant planets.

This work was supported in part by Grants-in-Aid for Scientific Research from the MEXT of Japan (15740118, 16077202, 18540238, 18740104, 20540238, and 21740136).

REFERENCES

- André, P., Basu, S., & Inutsuka, S. 2008. in *Structure Formation in Astrophysics*, ed. G. Chabrier (Cambridge: Cambridge University Press), 254

- Banerjee, R., & Pudritz, R. E. 2006, *ApJ*, 641, 949
- Durisen, R. H., et al. 2007, in *Protostars and Planets V*, ed. B. Reipurth, D. Jewitt, & K. Keil (Tucson, AZ: Univ. Arizona Press) 607
- Gammie, C. F. 2002, *ApJ* 553, 174
- Greaves, J. S, Richards, A. M. S., Rice, W. K. M., & Muxlow, T. W. B. 2008, *MNRAS* 391, L74
- Hennebelle, P. & Fromang, S. 2008 *A&A*, 477, 9
- Hori, Y. & Ikoma, M. (2008) *ApJ* 714, 1343
- Hubickyj, O., Bodenheimer, P., & Lissauer, J. J. 2005, *Icarus* 179, 415
- Ida, S. & Lin, D. N. C. 2004, *ApJ* 616, 567
- Ikoma, M., Nakazawa, K., & Emori, H. 2000, *ApJ* 537, 1013
- Kalas, P. et al. 2008 *Science*, 322, 1345
- Kokubo, E., & Ida, S. 2002, *ApJ*, 581, 666
- Lagrange, A.-M. et al. 2008 *A&A* 493, L21
- Larson, R. B. 1969, *MNRAS*, 145, 271
- Lissauer, J. J., Hubickyj, O., D'Angelo, G. & Bodenheimer, P. 2009, *Icarus* 199, 338
- Machida, M. N., Matsumoto, T., Tomisaka, K., & Hanawa, T. 2005, *MNRAS*, 362, 369
- Machida, M. N., Inutsuka, S., & Matsumoto, T. 2006a, *ApJ* 647, L151
- Machida, M. N., Inutsuka, S., & Matsumoto, T. 2007, *ApJ* 670, 1198
- Machida, M. N., Inutsuka, S., & Matsumoto, T. 2008a, *ApJ* 676, 1088
- Machida, M. N., Kokubo, E., Inutsuka, S., & Matsumoto, T. 2010, *MNRAS* 405, 1227
- Machida, M. N., Matsumoto, T., Hanawa, T., & Tomisaka, K. 2006b, *ApJ*, 645, 1227
- Machida, M.N., Tomisaka, K., Matsumoto, T. & Inutsuka, S. 2008c *ApJ* 677, 327
- Machida, M. N., Inutsuka, S., & Matsumoto, T. 2009, *ApJ* 704, L10
- Marois, C. et al. 2008 *Sci*, 322, 1348

- Masunaga, H., & Inutsuka, S. 2000, ApJ 531, 350
- Masunaga, H., Miyama, S. M., & Inutsuka, S. 1998, ApJ 495, 346
- Muto, T. & Inutsuka, S. 2009 ApJ 695, 1132
- Nakano, T., Nishi, R., & Umebayashi, T. 2002, ApJ 573, 199
- Pollack, J. B., Hubickyj, O., Bodenheimer, P., Lissauer, J. J., Podolak, M., & Greenzweig, Y. 1996, Icarus, 124, 62
- Rice, W. K. M., et al. 2003, MNRAS 346, L36
- Rice, W. K. M., Lodato, G., & Armitage, P. J. 2005, MNRAS 364, L56
- Thalmann, C. et al. 2009 ApJ 707, L123
- Tomisaka, K. 2002 ApJ 575, 306
- Wardle, M., & Ng, C. 1999, MNRAS, 303, 239
- Winkler, K.-H. A., & Newman, M. J. 1980a, ApJ, 236, 201
- Winkler, K.-H. A., & Newman, M. J. 1980b, ApJ, 238, 311